Journal of Solid State Chemistry 182 (2009) 1217–1221

Contents lists available at ScienceDirect

Journal of Solid State Chemistry

journal homepage: www.elsevier.com/locate/jssc

Comparative XANES study on the two electron-doped high-T_c superconductor systems, (Sr,La)CuO_2 and $(Nd,Ce)_2CuO_4$

Y. Tanaka [a], M. Karppinen [a,b,*], J.M. Chen [c], R.S. Liu [d], H. Yamauchi [a,b]

[a] Materials and Structures Laboratory, Tokyo Institute of Technology, Yokohama 226-8503, Japan
[b] Laboratory of Inorganic Chemistry, Department of Chemistry, Helsinki University of Technology, FI-02015 TKK, Finland
[c] National Synchrotron Radiation Research Center, Hsinchu 30076, Taiwan, ROC
[d] Department of Chemistry, National Taiwan University, Taipei 106, Taiwan, ROC

ARTICLE INFO

Article history:
Received 4 October 2008
Received in revised form
13 January 2009
Accepted 6 February 2009
Available online 21 February 2009

Keywords:
High-T_c superconductivity
Electron doping
XANES spectroscopy
Infinite-layer structure
T'structure

ABSTRACT

Here we employ high-quality samples of $(Sr_{1-x}La_x)CuO_2$ and $(Nd_{2-x}Ce_x)CuO_4$ and XANES spectroscopy at O-*K*, Cu-$L_{2,3}$ and Ce-$M_{4,5}$ edges to gain comprehensive understanding of the electronic structure and doping in *n*-type high-T_c superconductors. Not only common but also slightly different features are revealed for the two systems. From O-*K*-edge spectra, the UHB is found essentially independent of the electron-doping level for both the systems, in line with our understanding that the doped electrons do not go to the O site in *n*-type copper-oxide superconductors. Another common observation is that the main Cu^{II} peak at the Cu-L_3 edge (due to transitions to the Cu^{II}-3*d* orbitals) systematically decreases in intensity upon electron doping, hence verifying the fact that the doped electrons go to the Cu site. The difference then between the two systems is that in $(Sr_{1-x}La_x)CuO_2$ the weaker Cu^{II} peak due to transitions to the Cu^{II}-4*s* orbital depends on the degree of doping. Moreover, it was found that with increasing *x*, electron density increases much faster in $(Sr_{1-x}La_x)CuO_2$ than in $(Nd_{2-x}Ce_x)CuO_4$. This is a consequence of two phenomena: a tiny increase in oxygen content concomitant to the Ce^{IV}-for-Nd^{III} substitution and the somewhat lower Ce-valence value of +3.8 compared to the nominal tetravalent state.

1. Introduction

To date only two electron-doped (*n*-type) high-T_c superconductive copper-oxide systems, i.e. (Sr,*R*)CuO_2 [1] and $(R,Ce)_2CuO_4$ [2] (*R* = La, Pr, Nd, etc.), have been identified. Both possess the two-dimensional apical-oxygen-free CuO_2 plane in which copper is in a square-planar coordination with a valence value lower than +2. In the so-called infinite-layer structure of the (Sr,*R*)CuO_2 system, the CuO_2 plane is stacked with a single (Sr,*R*) cation layer, whereas in the so-called T' structure of the $(R,Ce)_2CuO_4$ system it is combined to the fluorite-structured (*R*,Ce)–O_2–(*R*,Ce) block. In both the systems, occurrence of superconductivity requires (i) highly reductive synthesis/post-annealing conditions and (ii) an appropriate amount of electrons doped into the CuO_2 plane through the higher-for-lower-valence cation substitution, i.e. R^{III}-for-Sr^{II} for (Sr,*R*)CuO_2 and Ce^{IV}-for-R^{III} for $(R,Ce)_2CuO_4$ [3–5]. In comparison to the hole-doped (*p*-type) high-T_c superconductive copper-oxide systems much less is known about the *n*-type systems in regards to the carrier doping, superconductivity phase diagram and electronic structure.

X-ray absorption near-edge structure (XANES) spectroscopy at O-*K* and Cu-$L_{2,3}$ absorption edges provides us with a way to probe the local densities of unoccupied O 2*p* and Cu 3*d* states near the Fermi level in a site-selective manner and to quantitatively analyze the CuO_2-plane charge densities. There are a number of quantitative O-*K*-edge and Cu-$L_{2,3}$-edge XANES studies reported for various *p*-type high-T_c copper-oxide superconductor systems [6–18], but only a few on the two *n*-type copper-oxide superconductor systems, (Sr,*R*)CuO_2 [19] and $(R,Ce)_2CuO_4$ [20]. Moreover, these studies do not cover wide doping ranges, probably due to the apparent difficulties in sample synthesis once it comes to high-quality samples. Recently we collected O-*K*-edge and Cu-$L_{2,3}$-edge XANES data for an extensive number of high-quality samples of (Sr,La)CuO_2 and $(Nd,Ce)_2CuO_4$ with systematically increased electron-doping levels [21,22]. In the present contribution these data—analyzed in a consistent manner—are compared and discussed together. The results reveal both common and slightly different features of electronic structure and doping for the two systems. Moreover, Ce-$M_{4,5}$-edge XANES data are utilized to explain why in the $(Nd,Ce)_2CuO_4$ system the Ce^{IV}-for-Nd^{III} substitution induces electron densities lower than the La^{III}-for-Sr^{II} substitution does in the (Sr,La)CuO_2 system. Here the explanation is the lower-than-assumed valence value of Ce, i.e. +3.8.

* Corresponding author at: Laboratory of Inorganic Chemistry, Department of Chemistry, Helsinki University of Technology, FI-02015 TKK, Finland.
Fax: +358 9 462 373.
E-mail address: maarit.karppinen@tkk.fi (M. Karppinen).

0022-4596/$ - see front matter © 2009 Elsevier Inc. All rights reserved.
doi:10.1016/j.jssc.2009.02.014

2. Experimental

The two series of samples employed in the present work, i.e. $(Sr_{1-x}La_x)CuO_2$ ($0.00 \leqslant x \leqslant 0.10$) and $(Nd_{2-x}Ce_x)CuO_4$ ($0.00 \leqslant x \leqslant 0.20$), consisted of essentially single-phasic samples only . In both cases the precursor powder was prepared by employing a wet-chemical route in which the solution-mixed metal ions are uniformly bound by EDTA (ethylenediaminetetraacetic acid) into a gel which is then burned to obtain precursor ash. In the case of $(Sr_{1-x}La_x)CuO_2$ samples, the raw ash was fired in air at 950 °C for 72 h with several intermediate grindings prior to the actual synthesis carried out at 3 GPa and 700–1000 °C for 1 h in a cubic-anvil-type high-pressure (HP) apparatus. For the HP synthesis the precursor powder was loaded in a gold capsule together with Ti foils at the top and the bottom of the packed powder; the function of the Ti foils was to create the reductive atmosphere required for a successful synthesis [21]. The synthesis yielded high-quality samples with only a trace of an impurity phase, i.e. an unknown phase for $x \leqslant 0.075$ and $(La,Sr)_2Cu_2O_5$ for $x = 0.10$. In the case of $(Nd_{2-x}Ce_x)CuO_4$ samples, the precursor ash was pressed into pellets and fired in air at 1050 °C for 12 h. This yielded XRD-pure but not superconductive samples, as expected from previous studies [4]. In order to render the $(Nd_{2-x}Ce_x)CuO_4$ samples superconducting, they were annealed at 1000 °C for 24 h under an oxygen partial pressure, $P_{O_2} \approx 3.2 \times 10^{-4}$ atm for samples with $x \leqslant 0.06$ and $P_{O_2} \approx 1.0 \times 10^{-4}$ atm for those with $x \geqslant 0.065$. The P_{O_2} level applied was carefully determined for each cation composition so as to achieve the highest possible T_c value [23]. As described in detail in previous studies [5,23], the function of the reductive annealing is to eliminate the Cu vacancies existing in small concentration (1–2%) in as-air-synthesized $(Nd_{2-x}Ce_x)CuO_4$ samples. Note that at the same time it creates a trace of $(Nd,Ce)_2O_3$ as a secondary phase through the phase segregation of $(Nd,Ce)_2Cu_{1-y}O_4$ yielding a phase mixture: $(1-y)$ $(Nd,Ce)_2CuO_4$+y $(Nd,Ce)_2O_3$. The $(Nd,Ce)_2O_3$ trace is believed to be a rather inherited component of superconductive $(Nd,Ce)_2CuO_4$ samples [5,23].

The O-*K*-edge, Cu-$L_{2,3}$-edge and Ce-$M_{4,5}$-edge XANES measurements were carried out at the 6-m HSGM beam-line of National Synchrotron Radiation Research Center in Hsinchu, Taiwan, in a non-surface-sensitive X-ray fluorescence-yield mode for the O-*K*-edge and Cu-$L_{2,3}$-edge absorption and in an electron-yield mode for the Ce-$M_{4,5}$-edge absorption. The monochromator resolution was set to ~0.22, ~0.45 and ~0.4 eV for the O-*K*-edge, Cu-*L*-edge and Ce-*M*-edge energy regions, respectively. The recorded spectra were corrected for the energy-dependent incident photon intensity as well as for self-absorption effects and normalized to the tabulated standard absorption cross sections. Experimental details are found elsewhere [13,18,21,22].

All the samples were characterized for phase purity and lattice parameters by X-ray powder diffraction (XRD; Rigaku RINT 2000 equipped with a rotating Cu anode); the diffraction patterns have been presented in Refs. [21,22]. Based on the XRD all the samples studied here are of very high quality. The samples were also characterized for their superconductivity properties using a SQUID magnetometer (Quantum Design: MPMS-XL). The applied magnetic field was 10 Oe, and the T_c value was defined at the onset temperature of diamagnetic signal. Superconducting volume fraction was estimated from field-cooled magnetization at 5 K.

3. Results and discussion

We start the comparison of the two systems, $(Sr_{1-x}La_x)CuO_2$ and $(Nd_{2-x}Ce_x)CuO_4$, from their slightly different structural responses upon doping. In Fig. 1, lattice parameters, determined on the basis of XRD data in space group *P*4/*mmm* for the former

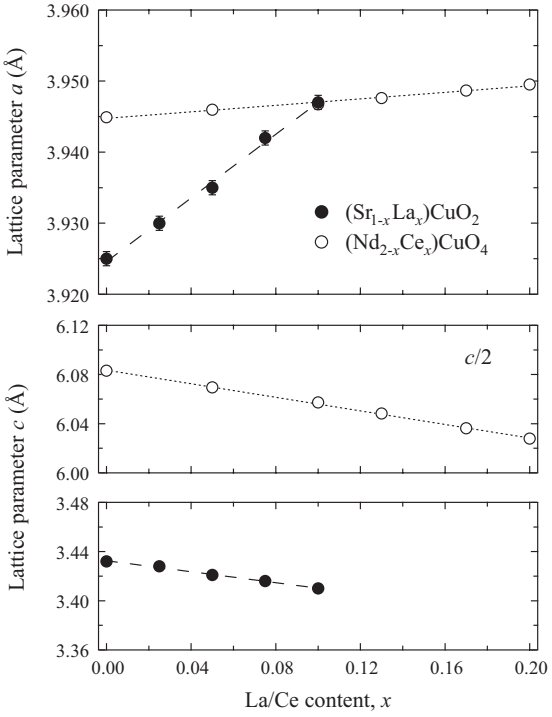

Fig. 1. Lattice parameters, *a* and *c* (or *c*/2), plotted against the substitution level, *x*, for the $(Sr_{1-x}La_x)CuO_2$ and $(Nd_{2-x}Ce_x)CuO_4$ samples. Note that the estimated errorbars are smaller than the symbol marks.

samples and in *I*4/*mmm* for the latter ones, are plotted against the substitution level, *x*. For both the systems, the *a* parameter linearly increases and the *c* parameter linearly decreases with increasing *x*. The increase in *a* is due to the electron-doping effect (into the antibonding Cu–O orbitals of the CuO_2 plane) while the decrease in *c* is explained by the smaller-for-larger cation substitution, i.e. La^{III} (1.16 Å) for Sr^{II} (1.26 Å) and Ce^{IV} (0.97 Å) for Nd^{III} (1.11 Å) [24]. For the two systems the average ionic radius, $r(Sr^{II}_{1-x}La^{III}_x)$ or $r(Nd^{III}_{2-x}Ce^{IV}_x)$, decreases nearly at the same rate with increasing *x* as also does the *c*-axis length. The expansion of *a* with increasing *x*, on the other hand, shows quite different rates for the two systems: for $(Sr_{1-x}La_x)CuO_2$ *a* increases by ~0.56% but for $(Nd_{2-x}Ce_x)CuO_4$ only by ~0.05% when *x* increases from 0.00 to 0.10. This difference may be related with the rather rigidly bound fluorite-structured $(Nd,Ce)_2O_2$ block between adjacent CuO_2 planes in $(Nd_{2-x}Ce_x)CuO_4$ that efficiently hinders the *a*-axis expansion. This thus either hinders the Cu–O bond expansion or makes the CuO_2 plane buckled. We suspect that here is a reason for the large difference in the "so-far maximized" T_c values of the two systems, i.e. 43 K for $(Sr_{1-x}La_x)CuO_2$ (with flat CuO_2 planes) and 24 K for $(Nd_{2-x}Ce_x)CuO_4$ (with presumably somewhat buckled CuO_2 planes). Also note that in $(Nd_{2-x}Ce_x)CuO_4$ the aliovalent Ce^{IV}-for-Nd^{III} substitution produces fewer electrons than expected since the actual valence of cerium is not exactly +4 but less (cf. the Ce-$M_{4,5}$-edge XANES data discussed later in this contribution).

Next we discuss the O-*K*-edge XANES spectra of the two systems. The pre-edge energy region, 526–532 eV, of the spectra is shown for representative $(Sr_{1-x}La_x)CuO_2$ and $(Nd_{2-x}Ce_x)CuO_4$ samples in Fig. 2. For both the systems the broad peak due to transitions into O 2*p* states hybridized with the UHB [8,13–15,20,25] is seen at ~529 eV. For $(Sr_{1-x}La_x)CuO_2$ the peak remains essentially unchanged independently of *x*, whereas for $(Nd_{2-x}Ce_x)CuO_4$ it systematically gains intensity and gets broader with increasing Ce-substitution level. The latter changes are, however, believed to be due to the Ce 5*d* and/or Ce 4*f* states

hybridized with the O 2*p* states [20,26], such that the UHB is in fact independent of the electron-doping level. Hence, we may conclude that the doped electrons do not go to the O site, and moreover, that the Fermi level is located at the bottom of the UHB in the *n*-type high-T_c superconductors [27,28].

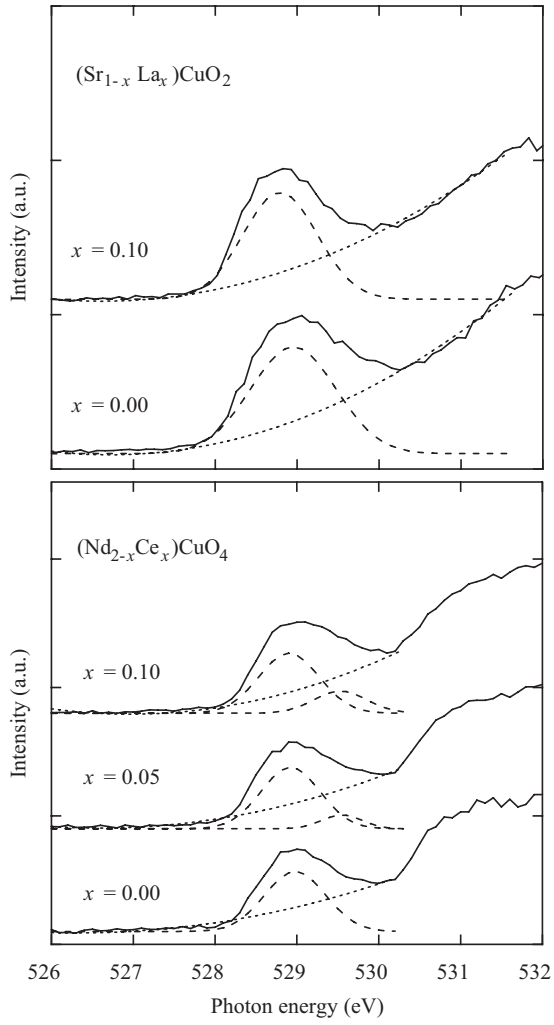

Fig. 2. Representative O-*K*-edge XANES spectra for the $(Sr_{1-x}La_x)CuO_2$ and $(Nd_{2-x}Ce_x)CuO_4$ samples. The broken lines illustrate the evolution of an additional feature about 529.5 eV for the latter system upon Ce-substitution.

Fig. 3 displays the Cu-$L_{2,3}$-edge absorption spectra for the two sample series, $(Sr_{1-x}La_x)CuO_2$ and $(Nd_{2-x}Ce_x)CuO_4$. The main peaks at the L_3 and L_2 edges (about 932 and 952 eV, respectively) are due to formally divalent copper states, Cu^{II}, i.e. transitions from the Cu $(2p_{3/2,1/2})3d^9$ ground state to the Cu $(2p_{3/2,1/2})^{-1}3d^{10}$ excited state, where $(2p_{3/2,1/2})^{-1}$ denotes a $2p_{3/2,1/2}$ hole [8]. For all the present samples these peaks are symmetric, indicating the absence of Cu^{III} states; note that oxidation of copper beyond +2 would create shoulders on the higher-energy sides of the main peaks [6–18]. Common to both the systems, the main peaks systematically lose intensity with increasing *x*, which indicates that the doped electrons are directed into the Cu site in *n*-type copper-oxide superconductors. For the $(Nd_{2-x}Ce_x)CuO_4$ system also seen is that the main peaks concomitantly shift to the higher energy direction (Figs. 3 and 4). Judging from the fact that no such peak-shift is seen in $(Sr_{1-x}La_x)CuO_2$, we tend to believe that it is not due to electron doping. Actually, Alexander et al. [25] have proposed based on their EELS data that the peak shift could be due to the potential of Ce^{IV} ions or a change in the Madelung potential about the Cu^{II} ions by the charge of Ce^{IV} ions.

From Fig. 3, it is also clear that in the L_3 area the absorption intensity systematically increases about 934 eV (for $(Sr_{1-x}La_x)CuO_2$ at ~933.7 eV and for $(Nd_{2-x}Ce_x)CuO_2$ at 933.9–934.5 eV) with increasing *x*. From a single spectrum only it would be difficult to distinguish this peak from the weak Cu^{II} peak at 936–937 eV (which is due to the transition to the Cu $(2p_{3/2})^{-1}3d^94s$ excited state [29]), but it becomes possible once we look at the development of the peak with increasing *x*. Since the ~934 eV peak is a common feature not only for the two *n*-type copper-oxide superconductor systems but also for other copper oxides with the valence of Cu lower than +2, e.g. Cu_2O [30] and $CuBa_2RCu_2O_6$ [8,13], we conclude that it is due to nominally monovalent Cu species, i.e. transitions from the Cu $(2p_{3/2})3d^{10}$ ground state to the Cu $(2p_{3/2})^{-1}3d^{10}4s$ excited state.

In order to gain quantitative information about the CuO_2 plane electron densities in the *n*-type copper-oxide superconductor systems, we analyzed the spectral features in the Cu-L_3-edge region by fitting the peaks at ~931.5 (main peak; due to Cu^{II}; transitions to 3*d* orbitals), ~934 (due to Cu^{I}) and 936–937 eV (due to Cu^{II}; transitions to 4*s* orbital) with combined Lorentzian and Gaussian functions, after approximating the background with a straight line (see the inset in Fig. 3). The results are given in

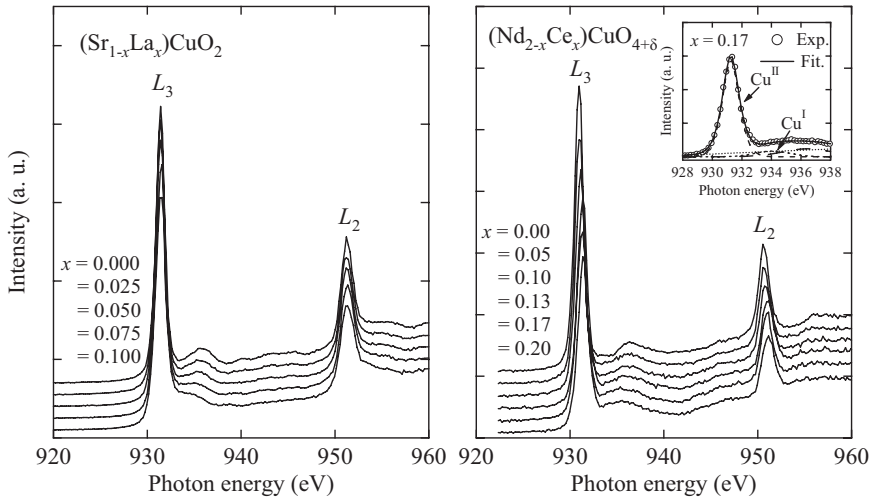

Fig. 3. Cu-$L_{2,3}$-edge XANES spectra for the $(Sr_{1-x}La_x)CuO_2$ and $(Nd_{2-x}Ce_x)CuO_4$ samples. The inset illustrates the fitting of the spectral features about the L_3 edge into Cu^{I} and Cu^{II} components for the $(Nd_{2-x}Ce_x)CuO_4$ sample with $x = 0.17$.

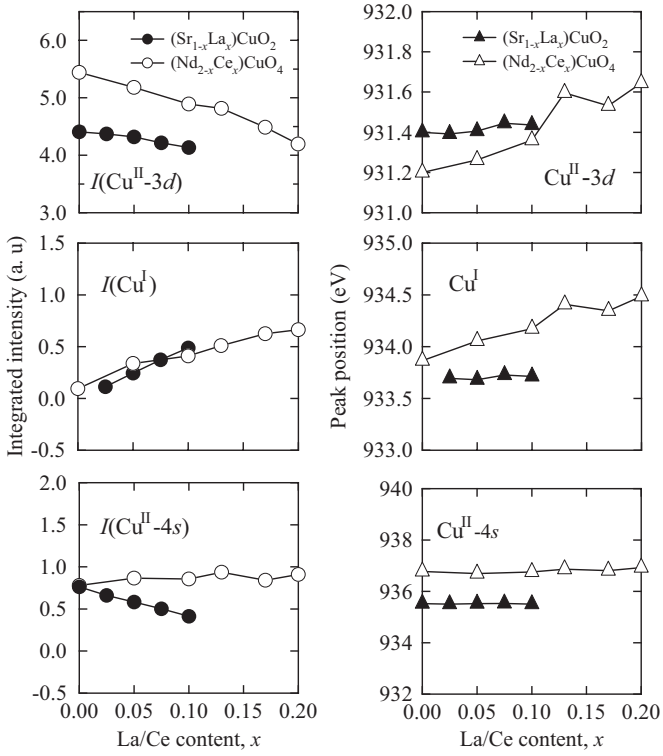

Fig. 4. Fitted intensities and the exact peak positions of the peaks in the Cu-L_3-edge XANES spectra for the $(Sr_{1-x}La_x)CuO_2$ and $(Nd_{2-x}Ce_x)CuO_4$ samples. Note that the estimated error-bars for both the integrated intensity and the peak position are smaller than the symbol marks.

Fig. 4. The integrated intensities of the three peaks at ~931.5, ~934 and 936–937 eV, i.e. $I(Cu^{II}\text{-}3d)$, $I(Cu^{I})$ and $I(Cu^{II}\text{-}4s)$, respectively, show clearly different trends for the two systems. Most profoundly, with increasing substitution level x, $I(Cu^{II}\text{-}3d)$ decreases strongly but $I(Cu^{II}\text{-}4s)$ remains constant in $(Nd_{2-x}Ce_x)CuO_4$, whereas for the $(Sr_{1-x}La_x)CuO_2$ system both $I(Cu^{II}\text{-}3d)$ and $I(Cu^{II}\text{-}4s)$ decrease moderately. Hence, we conclude that the electronic structures may not be exactly identical for the two n-type high-T_c superconductor systems.

From the fitting results we calculated an estimate for the valence of copper with $V(Cu)\equiv 2-I(Cu^{I})/[I(Cu^{I})+I(Cu^{II}\text{-}3d)]$. In Fig. 5, the resultant V(Cu) value is plotted against x for the two systems, $(Sr_{1-x}La_x)CuO_2$ and $(Nd_{2-x}Ce_x)CuO_4$. It is seen that for both the systems, V(Cu) decreases linearly with x, but the rate of decrease is quite different for them; in $(Sr_{1-x}La_x)CuO_2$ V(Cu) decreases much faster than in $(Nd_{2-x}Ce_x)CuO_4$. This difference may be explained with the fact that in $(Nd_{2-x}Ce_x)CuO_4$ the effect of Ce^{IV}-for-Nd^{III} substitution is partially counteracted by a concomitant small increase in oxygen content as was demonstrated through accurate wet-chemical redox analysis in Ref. [23], whereas in $(Sr_{1-x}La_x)CuO_2$ oxygen content presumably remains essentially constant upon La^{III}-for-Sr^{II} substitution. Moreover, the valence of cerium, V(Ce), in $(Nd_{2-x}Ce_x)CuO_4$ seems to be somewhat lower than the nominally assumed value of +4 based on the Ce-$M_{4,5}$ XANES data [22]. For all our $(Nd_{2-x}Ce_x)CuO_4$ samples the spectrum at the Ce-M_4 and M_5 areas is composed of a main peak together with its low-energy shoulder. Such features have been interpreted as signatures of tetravalent and trivalent cerium, respectively [31,32]. In Fig. 6 a representative spectrum is shown (for $x = 0.10$) together with a spectrum for a CeO_2 reference (which lacks the shoulder peaks due to trivalent cerium). Quantitative estimates for the valence of cerium in our $(Nd_{2-x}Ce_x)CuO_4$ samples were obtained by fitting the spectral

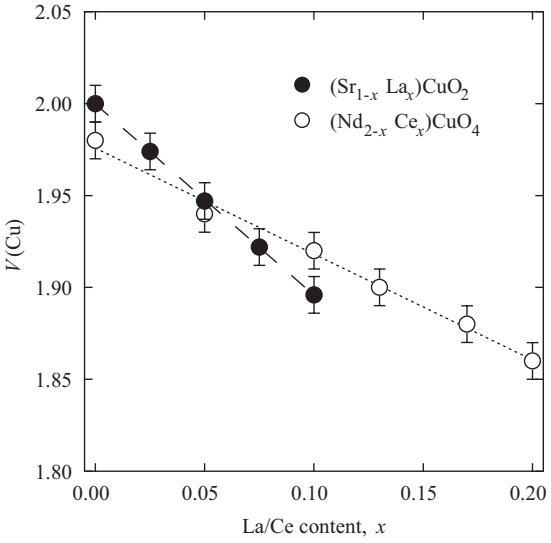

Fig. 5. Valence of copper, V(Cu), as estimated from the Cu-L_3-edge XANES data with respect to the substitution level, x, for the $(Sr_{1-x}La_x)CuO_2$ and $(Nd_{2-x}Ce_x)CuO_4$ samples.

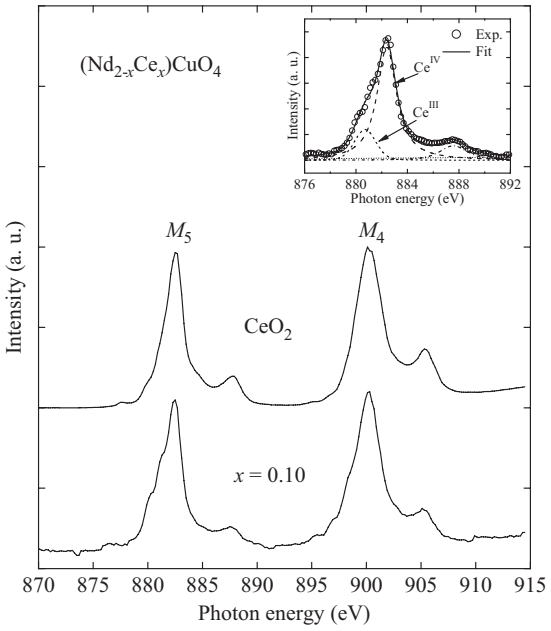

Fig. 6. Ce-$M_{4,5}$-edge XANES spectra for a $(Nd_{2-x}Ce_x)CuO_4$ sample with $x = 0.10$ and a CeO_2 reference. The inset illustrates the fitting of the spectral features about the M_5 edge into Ce^{III} and Ce^{IV} components.

features about the Ce-M_5 edge (see the inset of Fig. 6); the V(Ce) values were then calculated from the intensities of the main peak due to tetravalent cerium $[I(Ce^{IV})]$ and its low-energy shoulder due to trivalent cerium $[I(Ce^{III})]$, as follows: $V(Ce)\equiv 4-I(Ce^{III})/[I(Ce^{III})+I(Ce^{IV})]$. For all our $(Nd_{2-x}Ce_x)CuO_4$ samples, such analysis yielded V(Ce) values close to +3.8.

Finally we discuss and compare the superconductivity characteristics of the two n-type high-T_c superconductor systems. In Fig. 7, the T_c values and superconducting volume fractions are plotted against the CuO_2-plane electron density defined by $n(CuO_2)\equiv 2-V(Cu)$. In both the systems, with increasing $n(CuO_2)$ value superconductivity suddenly appears with the maximum T_c value but the superconducting volume fraction increases more sluggishly with $n(CuO_2)$. Moreover, it was found from Fig. 7 that the largest superconducting volume fraction and the maximum T_c

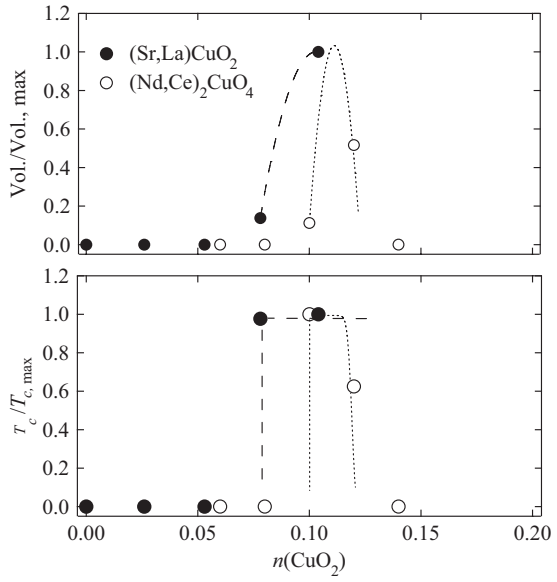

Fig. 7. Relationships between the superconductivity properties (T_c value and superconducting volume fraction) and the CuO_2-plane electron density, $n(CuO_2)$, for the $(Sr_{1-x}La_x)CuO_2$ and $(Nd_{2-x}Ce_x)CuO_4$ systems.

value are simultaneously achieved nearly at the same $n(CuO_2)$ value of 0.10–0.12 for both the systems. (The fact that the superconductivity characteristics of the $(Sr_{1-x}La_x)CuO_2$ system get rapidly worsen for $x>0.10$ has been well demonstrated in earlier studies [33,34].)

4. Conclusions

We have studied an extensive series of high-quality samples of the only *n*-type copper-oxide superconductor systems known to date, i.e. $(Sr_{1-x}La_x)CuO_2$ and $(Nd_{2-x}Ce_x)CuO_4$, and systematically characterized them by means of XANES spectroscopy at O-*K*, Cu-$L_{2,3}$ and Ce-$M_{4,5}$ edges in order to quantitatively probe the site-specific electron densities and to gain insights into the electronic structures of electron-doped high-T_c superconductors. Regarding the latter goal, both common and slightly different features were revealed for the two systems. From the O-*K*-edge XANES spectra, the UHB was found essentially independent of the electron-doping level for both the systems, indicating that the doped electrons do not go to the O site and, thereby, that the Fermi level is located at the bottom of the UHB in *n*-type high-T_c superconductors. Another feature common to both the systems is that the main peak of the Cu-L_3-edge region due to transitions to the Cu^{II}-3*d* orbitals systematically loses intensity upon electron doping. This verifies that the doped electrons go to the Cu site in *n*-type high-T_c superconductors. At the same time the two systems, $(Sr_{1-x}La_x)CuO_2$ and $(Nd_{2-x}Ce_x)CuO_4$, were found to differ from each other in terms of the Cu^{II}-4*s* peak which in the former system loses intensity upon electron doping while remaining unaffected in the latter. Regarding the electron densities, it was found that the $n(CuO_2)$ value increases more slowly in $(Nd_{2-x}Ce_x)$-CuO_4 than in $(Sr_{1-x}La_x)CuO_2$. This was explained as follows. First, the $(Nd_{2-x}Ce_x)CuO_4$ structure allows oxygen nonstoichiometry and accordingly the aliovalent Ce^{IV}-for-Nd^{III} substitution is partially counteracted by a concomitant small increase in oxygen content. Second, the valence of cerium was revealed on the basis of Ce-M_5-edge XANES spectra to be somewhat lower than assumed, i.e. +3.8. Finally, despite the small differences in electronic structure and doping efficiency, the $n(CuO_2)$ value at which the highest T_c value and the largest superconductivity volume fraction are achieved, was found almost the same for the two systems, being at 0.10–0.12 for both $(Sr_{1-x}La_x)CuO_2$ and $(Nd_{2-x}Ce_x)CuO_4$.

Acknowledgments

This work was partly supported by Tekes (no. 1726/31/07) and Academy of Finland (no. 116254).

References

[1] M.G. Smith, A. Manthiram, J. Zhou, J.B. Goodenough, J.T. Markert, Nature 351 (1991) 549.
[2] Y. Tokura, H. Takagi, S. Uchida, Nature 337 (1989) 345.
[3] G. Er, Y. Miyamoto, F. Kanamaru, S. Kikkawa, Physica C 181 (1991) 206.
[4] H. Takagi, S. Uchida, Y. Tokura, Phys. Rev. Lett. 62 (1989) 1197.
[5] H.J. Kang, P. Dai, B.J. Campbell, P.J. Chupas, S. Rosenkranz, P.L. Lee, Q. Huang, S. Li, S. Komiya, Y. Ando, Nat. Mater. 6 (2007) 224.
[6] A.Q. Pham, F. Studer, N. Merrien, A. Maignan, C. Michel, B. Raveau, Phys. Rev. B 48 (1993) 1249.
[7] N. Merrien, L. Coudrier, C. Martin, A. Maignan, F. Studer, A.M. Flank, Phys. Rev. B 49 (1994) 9906.
[8] N. Nücker, E. Pellegrin, P. Schweiss, J. Fink, S.L. Molodtsov, C.T. Simmons, G. Kaindl, W. Frentrup, A. Erb, G. Müller-Vogt, Phys. Rev. B 51 (1995) 8529.
[9] E. Pellegrin, J. Fink, C.T. Chen, Q. Xiong, Q.M. Lin, C.W. Chu, Phys. Rev. B 53 (1996) 2767.
[10] M. Merz, N. Nücker, P. Schweiss, S. Schuppler, C.T. Chen, V. Chakarian, J. Freeland, Y.U. Idzerda, M. Kläser, G. Müller-Vogt, Th. Wolf, Phys. Rev. Lett. 80 (1998) 5192.
[11] P. Ghigna, G. Spinolo, G. Flor, N. Morgante, Phys. Rev. B 57 (1998) 13426.
[12] M. Karppinen, M. Kotiranta, H. Yamauchi, P. Nachimuthu, R.S. Liu, J.M. Chen, Phys. Rev. B 63 (2001) 184507.
[13] M. Karppinen, H. Yamauchi, T. Nakane, K. Fujinami, K. Lehmus, P. Nachimuthu, R.S. Liu, J.M. Chen, J. Solid State Chem. 166 (2002) 229.
[14] M. Karppinen, M. Kotiranta, T. Nakane, H. Yamauchi, S.C. Chang, J.M. Chen, R.S. Liu, Phys. Rev. B 67 (2003) 134522.
[15] M. Karppinen, S. Lee, J.M. Lee, J. Poulsen, T. Nomura, S. Tajima, J.M. Chen, R.S. Liu, H. Yamauchi, Phys. Rev. B 68 (2003) 54502.
[16] M. Karppinen, Y. Morita, J.M. Chen, R.S. Liu, H. Yamauchi, Phys. Rev. B 72 (2005) 12501.
[17] M. Schneider, R.-S. Unger, R. Mitdank, R. Müller, A. Krapf, S. Rogaschewski, H. Dwelk, C. Janowitz, R. Manzke, Phys. Rev. B 72 (2005) 14504.
[18] M. Karppinen, Y. Morita, T. Kobayashi, I. Grigoraviciute, J.M. Chen, R.S. Liu, H. Yamauchi, J. Solid State Chem. 178 (2005) 3464.
[19] R.S. Liu, J.M. Chen, P. Nachimuthu, R. Gundakaram, C.U. Jung, J.Y. Kim, S.I. Lee, Solid State Commun. 118 (2001) 367.
[20] E. Pellegrin, N. Nücker, J. Fink, S.L. Molodsov, A. Gutiérrez, E. Navas, O. Strebel, Z. Hu, M. Domke, G. Kaindl, S. Uchida, Y. Nakamura, J. Markl, M. Klauda, G. Saemann-Ischenko, A. Krol, J.L. Peng, Z.Y. Li, R.L. Greene, Phys. Rev. B 47 (1993) 3354.
[21] Y. Tanaka, M. Karppinen, J.M. Lee, R.S. Liu, J.M. Chen, H. Yamauchi, Solid State Commun. 147 (2008) 370.
[22] Y. Tanaka, M. Karppinen, T. Kobayashi, T.S. Chan, R.S. Liu, J.M. Chen, H. Yamauchi, Chem. Mater. 20 (2008) 5414.
[23] Y. Tanaka, T. Motohashi, M. Karppinen, H. Yamauchi, J. Solid State Chem. 181 (2008) 365.
[24] R.D. Shannon, Acta Crystallogr. A 32 (1976) 751.
[25] M. Alexander, H. Romberg, N. Nücker, P. Adelmann, J. Fink, J.T. Markert, M.B. Maple, S. Uchida, H. Takagi, Y. Tokura, A.C.W.P. James, D.W. Murphy, Phys. Rev. B 43 (1991) 333.
[26] J. Fink, N. Nuecker, M. Alexander, H. Romberg, M. Knupfer, M. Merkel, P. Adelmann, R. Claessen, G. Mante, T. Buslaps, S. Harm, R. Manzke, M. Skibowski, Physica C 185–189 (1991) 45.
[27] Z. Tan, J.I. Budnick, C.E. Bouldin, J.C. Woicik, S.W. Cheong, A.S. Cooper, G.P. Espinosa, Z. Fisk, Phys. Rev. B 42 (1990) 1037.
[28] T. Takahashi, H. Katayama, H. Matsuyama, Z. Phys. B 78 (1990) 343.
[29] F.J. Flipse, G. van der Laan, A.L. Johnson, K. Kadowaki, Phys. Rev. B 42 (1990) 1997.
[30] M. Grioni, J.B. Goedkoop, R. Schoorl, F.M.F. de Groot, J.C. Fuggle, F. Schäfers, E.E. Koch, G. Rossi, J.-M. Esteva, R.C. Karnatak, Phys. Rev. B 39 (1989) 1541.
[31] G. Kalkowski, G. Kaindl, G. Wortmann, D. Lentz, S. Krause, Phys. Rev. B 37 (1988) 1376.
[32] S.O. Kucheyev, B.J. Clapsaddle, Y.M. Wang, T. van Buuren, A.V. Hamza, Phys. Rev. B 76 (2007) 235420.
[33] G. Er, S. Kikkawa, F. Kanamaru, Y. Miyamoto, S. Tanaka, M. Sera, M. Sato, Z. Hiroi, M. Takano, Y. Bando, Physica C 196 (1992) 271.
[34] N. Ikeda, Z. Hiroi, M. Azuma, M. Takano, Y. Bando, Y. Takeda, Physica C 210 (1993) 367.